Heliyon 10 (2024) e34093

Contents lists available at ScienceDirect

Heliyon

journal homepage: www.cell.com/heliyon

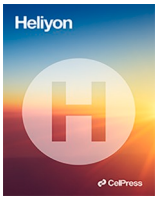

Research article

Integrated geophysical Investigation for gold mineralization potential over southern parts of Kebbi state and its Environs, northwestern Nigeria

K.A. Salako [a,*], A.A. Adetona [a], A.A. Rafiu [a], A.I. Augie [b], M.O. Jimoh [c], A. Alkali [a], R. A. Muriana [d], J.O. Lawrence [a]

[a] Department of Geophysics, Federal University of Technology Minna, Nigeria
[b] Department of Applied Geophysics, Federal University Birnin Kebbi, Nigeria
[c] Department of Geology, Federal University of Technology Minna, Nigeria
[d] Materials and Metallurgical Engineering Department, Federal University of Technology Minna, Nigeria

ARTICLE INFO

Keywords:
Potential mineralization zones
Gold mineralization
Structural features
Hydrothermal alteration zones
And airborne magnetic and radiometric techniques

ABSTRACT

The potential zones of gold mineralization were identified in this study using aeromagnetic and aero-radiometric methods. The Nigerian Geological Survey Agency (NGSA) provided half-degree airborne magnetic and radiometric datasets covering the southern part of Kebbi State. Magnetic data were subjected to first vertical derivative (1VD), total gradient amplitude (TGA), total horizontal derivative (THD), source edge detection (SED), center for exploration targeting (CET), Euler deconvolution (ED) and source parameter imaging (SPI) to identify favourable structures to gold mineralization. Aero-radiometric data delineation of the region of hydrothermal alteration zones through the K/eTh ratio, K_deviation, F_parameters, and Ternary image analyses were successful. The results of the magnetic data techniques revealed the regions of major structures/or lineaments with gold mineralization attributes, trending in the NE to SW directions and the SE to NE parts of the study area. The depth to the structures of the magnetic source hosting gold mineralization was less than 5 m using algorithm ED and SPI techniques. Normalized radiometric data showed the area of anomalously high and moderate hydrothermal altered zones. The region's designation as a gold field is supported by major fault lines observed on the 1VD, a sequence of bristle fractures from the CET analysis, and high values of K_deviation and F_parameter, all of which are were visible on the Ternary images. The integrated results revealed zones of major structures and hydrothermal regions of gold fields at Agwara, Western Magama, Rijau, Fakai, Bukkuyum, and Borgu in the SE of the study area.

1. Introduction

Mineral resource exploration is largely dependent on subsurface structural and hydrothermal alteration analyses [1]. According to Refs. [2–4] hydrothermally altered zones and structural focus have impacts on mineral deposits and hydrocarbon accumulations, either directly or indirectly. A geophysical method showing possible routes for mineral exploration is necessary since the structures in the Nigerian basement complexes are usually in control of mineralization and may be well-established [4]. With shear zones and

* Corresponding author.
E-mail address: s.kazeem@futminna.edu.ng (K.A. Salako).

https://doi.org/10.1016/j.heliyon.2024.e34093
Received 9 February 2024; Received in revised form 1 July 2024; Accepted 3 July 2024
Available online 4 July 2024

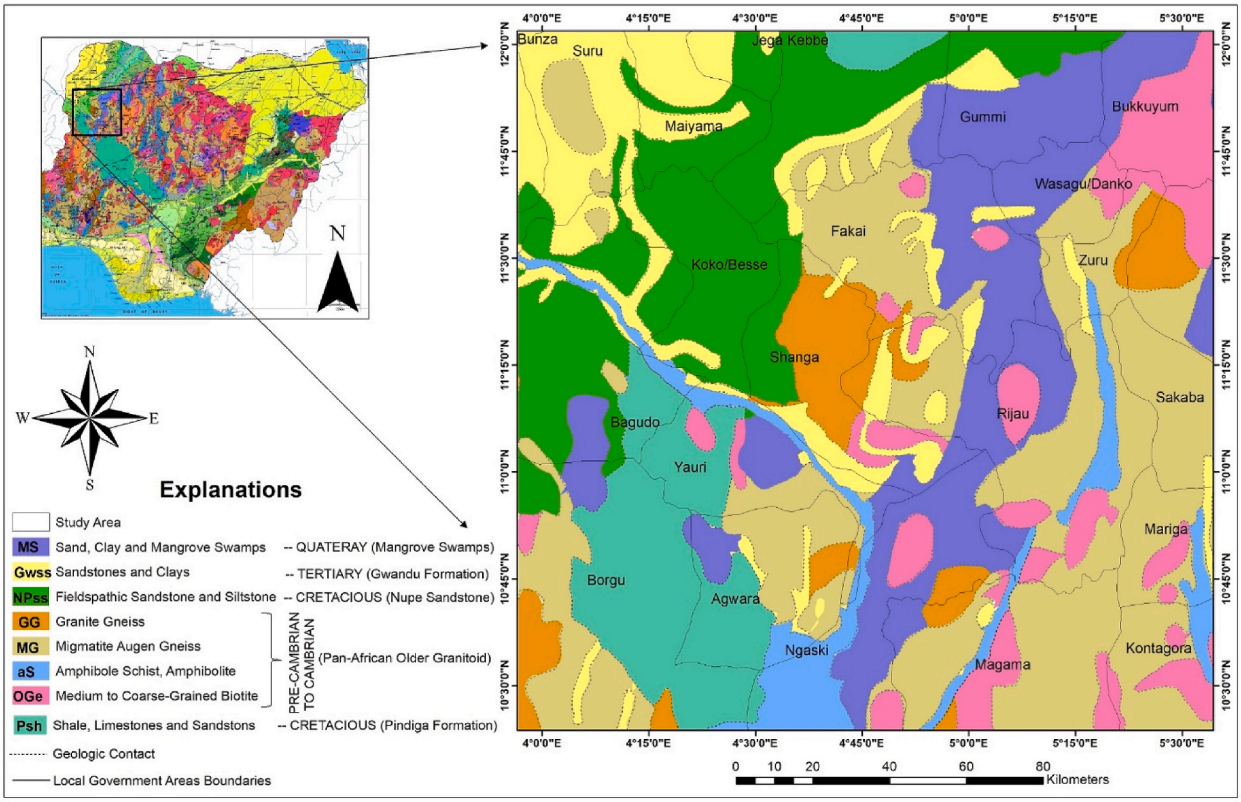

Fig. 1. Location and geological map of the study.

hydrothermal veins emerging in response to the regional stress field, most mineralized zones are structurally regulated and spatially connected [5,6]. Given that these structures might be shallow or deeply buried, a geophysical method is necessary to identify potential routes for gold exploration [6]. The structures such as fractures/shears and hydrothermally altered zones are important in the mineralization of gold because they act as both loci of mineralization fluid deposition and conduits for the mineralization solution [3].

Delineating structures such as faults, folds, contacts, shear zones, intrusions, and favourable areas for ore deposits are some of the roles of the aeromagnetic method in mineral exploration [7,8]. The aforementioned structures, which are often detectable by airborne magnetic techniques, are significant in determining the location of mineralization potential [9].

Several enhancement techniques can be employed to achieve the objectives of obtaining the structures associated with mineralization potential. Some of these techniques are the first vertical derivative "FVD" [10,11], tilt derivative "TDR" [12], horizontal gradient magnitude "HGM" [13–16], center for exploration targeting "CET" [17], and others. Additionally, automated techniques exist for identifying porphyry magnetic signatures and defining lineaments, which are used to pinpoint favourable ore deposit areas [18,19].

For aero-radiometric measurements, the variations in these radioelement (K, Th, U) concentrations between rocks allow for the mapping and characterization of the various lithological units [20–22]. The variations in these radioelement concentrations between rocks allow for the mapping and characterization of the various lithological units units [20–22].

Earlier geophysical studies include [23]: identified the alteration zones using Landsat ETM + images taken along the Garin Hawal shear zone. False-colour composite images were used in the study to reveal regional geologic mapping and structural analysis of the area. This detailed field and structural mapping had led to the delineation of gold-bearing alteration zones. However, the authors should have followed up the findings with other geophysical methods.

[24] analysed aeromagnetic data over the southern part of Kebbi State in northwest Nigeria to identify structural potential mineralization zones. The study involves the use of enhancement filters such as analytic signal (AS), first vertical derivatives (FVD), second vertical derivatives (SVD), and tilt derivatives (TDR). The results unanimously led to the delineation of NE-SW trending features such as fractures, faults, and veins within which economic minerals mostly settle. However, the gaps from the literature is that, most of the authors did not applied the magnetic equator filter technique to centralise the anomalies, because the study area falls within the low latitude area of the equatorial zones [19,25]. Similarly, most of their findings were not followed up with other geophysical methods.

Generally, the previous geophysical and geochemical studies in the region by Refs. [23,24,26–30]. revealed significant structural trends that extend from north to south and are consistent with the northwest-trending regional structural trend. The results also indicated that the basement complex is dominant in the region, which may contain commercial minerals. Significant geochemical

traits in some selected locations pointed to a primary distant hydrothermal source of mineralization [27].

However, the previous geophysical research in the area was limited, and additional geophysical techniques should be combined with the findings to confirm the obtained results. The novelty in this current research is use of centre for exploration targeting (CET) technique in conjunction with the Th/K ratio, F-parameter, and K-deviation techniques to reveal the hydrothermal alteration that usually harbours orogenic gold, which normally occurs within tectonically deformed crustal rocks that serve as conduits for hydrothermal fluids. According to studies conducted by Refs. [31,32], there is a correlation between potassium enrichment, thorium deprecation, and the gold mineralization process via the use of the hydrothermal indicator. Furthermore, the coordinates, locations, and geological setting of the areas with potential for gold mineralization were mapped out.

Likewise, the study area is low latitude, though, and the previous aeromagnetic studies should correctly have applied a reduction-to-equator (RTE) filter to centralise the anomalies [30,31]. This is due to the fact that at low latitudes, even with RTE-filtered data, a distinct amplitude needs to be corrected to prevent aberrant noise in the results of the north-south signal [19,25].

This study used high-resolution airborne magnetic and radiometric data, as well as the geological setting of the area, to delineate structural features, structure depth, and hydrothermal alteration zones that may host gold mineralization. The study aim was achieved by employing the following techniques for analysing aeromagnetic data: First Vertical Derivative (FVD), Total Gradient Amplitude (TGA), Total Horizontal Derivative (THD), Source Edge Detection (SED), Centre for Exploration Targeting (CET), and Source Parameter Imaging (SPI). Aero-radiometric data analyses techniques include K-deviation, Th/K ratio, F-parameter, and Ternary images. The results of these techniques reveal the zones of major geological structures (lineaments) such as faults, fractures, and shear zones, as well as hydrothermal alteration zones, which play a significant role in defining gold mineralized prospects.

The study area is located in southern Kebbi state, as well as parts of Zamfara and Niger States, between latitudes 10°30′0″N and 12°0′0″N, and longitudes 4°0′0″E and 5°30′0″E (Fig. 1). The region is located in the basement complex regions of northwest Nigeria, according to geology. These consist of the Pan-African Older Granitoid, Gwandu Formation, Nupe Sandstone, and Mangrove Swamps. As shown in Fig. 1, these included Sands, Clays, Fieldspathic Sandstones, Siltstones, Limestones, Mangrove Swamps, Medium to Coarse-Grained Biotite, Migmatitic Augen Gneiss, and Granite Gneiss. Furthermore, dacites/rhyolites overlie and intrude on the area's basement, which consists of gneisses, metasediments, and granitic rocks from Kebbi's southern (Anka-Yauri schist) part [33].

2. Methodology

The Nigeria Geological Survey Agency (NGSA) provided the aeromagnetic and aero-radiometric data set for the research area as Sheet 72 (Giru), 73 (Eokku), 74 (Donko), 95 (Kaoje), 96 (Shanga), 97 (Zuru), 117 (Konkwesso), 118 (Yelwa), and 119 (Chifu). Preprocessing of the magnetic data requires removal of offset, diurnal, and the International Geomagnetic Reference Field (IGRF). The survey parameters and data set specifications are detailed as "Source and Parameter for the Data".

Collected data has been being subjected to filters and mathematical algorithms contained in geophysical data processing software to enrich the data sets for clearer interpretation. The nine aeromagnetic data sheets were knitted together to generate a single map using the Oasis Montaj map knitting plugins. The essential filters used in research for evaluating mineralized structures include the creation of a total magnetic intensity map, the first vertical derivative, the analytic signal, the tilt derivative, and the centre for exploration targeting as well as algorithm ED and SPI with the aim of revealing structural features and depth that could host gold mineralization.

2.1. Data sources and data parameter

The data were collected under the following high-resolution survey conditions: Tie line spacing of 2000 m, terrain clearance of 80 m, flight line spacing of 500 m), flight direction of NW-SE, and tie line direction of NE-SW. The acquisition of the magnetic dataset involves the attachment of the 3 × 3 Scintrex CS3 Cesium magnetometer sensor to a fixed wing of the aircraft. This method measures the admixture of the earth's core field and the field due to magnetically susceptible rocks in the crust combined with the remanence field of the rocks.

The data were collected in a grid format which was further converted into a digitized form (X, Y and Z). The X and Y represent longitude and latitude respectively measured in meters [m] and Z represents the magnetic intensity measured in nanoteslas [nT].

The acquired data were corrected by removing the geomagnetic gradient (International Geomagnetic Reference Field, IGRF) using the main/core field. The magnetic anomaly (TMI anomaly) was calculated by subtracting the generated core fields (DGRF for the epoch period) from the grid values (TMI). The resulting Anomalous Magnetic Intensity Field (AMF) data was reduced to the magnetic equator in order to reveal an anomaly of the magnetized body that usually depends on the inclination, declination, local earth's field, and orientation of the body to magnetic north.

The obtained data were further processed, enhanced and interpreted by employing different processing techniques with the aid of Geosoft (Oasis Montaj), Arc GIS and Surfer using different and diverse filtering techniques in both time and frequency domains.

2.2. Theory of analysing tools

2.2.1. First vertical derivative technique

The vertical derivative of the field is intended to enhance the shallow features while attenuating the deep seated features and sharpen the shorter wavelength at the shallow subsurface region. The technique also observes the lateral variation of the susceptibility to map any sharp discontinuity within the field that could depict fracture or fault line [10,11]. Computing the 1VD could be angle

complex due to a simple fact that the study area lies within the equator where the angle of inclination is less than 15^0.

Note that at the equator, the vertical component of the magnetic field is $Z = TCos\theta$ where $\theta = 90^0$ this implies that $Z = 0$ at the equator, therefore, to evaluate the vertical derivative of the data, it needs to be taken to an imaginary pole, where $\theta = 0$, where the magnetic intensity is maximum, and the vertical derivative can be computed. Therefore, the IVD was computed on the total magnetic intensity anomaly reduction to equator (TMIA-RTE)

2.2.2. Total gradient amplitude (TGA) techniques

Total Gradient Amplitude (TGA) can be computed from the root mean square of the squared sum of the vertical and orthogonal derivatives of the anomalous magnetic field [15].

$$A(x,y) = \sqrt{\left((\partial T/\partial x)^2 + (\partial T/\partial y)^2 + (\partial T/\partial z)^2\right)} \tag{1}$$

where $A(x,y)$ constitute the amplitude of the total gradient of the signal at the (x,y) plane, T is the measured magnetic susceptibility, $\partial T/\partial x + \partial T/\partial y + \partial T/\partial z$ are the vertical and orthogonal derivatives along the z, y *and* x planes, respectively. (TGA) is devoid of ambient field and the direction of the source anomaly. A unique feature of this algorithm is in its ability placing the anomaly directly above the causative body, through vector resolution of the effect of the angle of inclination and declination on the magnetic data.

2.2.3. Total horizontal derivative (THD) techniques

As the name implies total horizontal derivative (THD) technique is very handy in observing the changes that occur to magnetic field at crustal depth due to contacts and other intrusive bodies. It is a fast and reliable method of estimating contact locations of causative bodies at shallow horizon. The input grids are the first-order derivatives of the field in the Cartesian coordinate [15,16,19].

$$THD(x,y) = \sqrt{\left((\partial T/\partial x)^2 + (\partial T/\partial y)^2\right)} \tag{2}$$

where T is the magnetic field intensity, $\partial T/\partial x$ and $\partial T/\partial y$ are its orthogonal derivative. This works on the assumption that the source anomaly is an isolated vertical thick dyke just as the regional nominal field. The THD technique was computed using the AMF that was Reduced to the Equator, it assumed that induced magnetization of the field sources are horizontal. This takes care of the regional field and source of magnetisations that are vertical.

2.2.4. Source edge detection (SED) technique

The source edge detection (SED) filter is achieved by employing the result from total horizontal derivative (THD) as input, it locates peaks from the THD data. In general, peaks observed on the SED filter align with the corresponding edges of magnetic sources, which in turn defines the geological contacts within an investigated area. The strike of the magnetic field anomalies are display in feathery-like symbol.

2.2.5. 3-D Euler deconvolution (ED) technique

The use of the Euler Deconvolution algorithm is aimed at achieving two primary purposes; delineating structures such as contact, and locating the source of an anomaly and its apparent depth. Its unique ability to perform regional residual filter to the source data, which enables the use of total field data and the versatile nature of the equation generated which can be filtered to obtain the desired result. A structural index of 1 was employed in generating the equations for the study area, adjustments were made to the channels *dxy* and the peak values until acceptable results that correlated with both the geology and other structures observed in the TGA and SED were obtained [34,35]. The 3-D standard Euler deconvolution technique relies on solving Euler's homogeneity equation (3) [35]:

$$(x - x_0)\frac{\partial T}{\partial x} + (y - y_0)\frac{\partial T}{\partial y} + (z - z_0)\frac{\partial T}{\partial z} = \eta(\beta - T) \tag{3}$$

where β is the magnetic field value and $\times_0$, y_0, z_0 the position of the anomaly, η, defines the structural index, is the most important parameter. Identified structural geometry and depth was controlled by the structural index; η [35}.

2.2.6. Source parameter imaging technique

The SPI method was utilised to differentiate and characterise deep magnetic source regions from shallow magnetic source regions, as well as to determine depth to magnetic source [34]. The depth estimate is unaffected by magnetic inclination, declination, dip, strike, or remanent magnetization [36]. The SPI technique assumes a step type source model [37] and the following formula holds:

$$Depth = \frac{1}{W_{max}} \tag{4}$$

where $W_{\max}$ represents the peak value of the local wavenumber (W) over the step source:

$$W = \sqrt{\left(\frac{dA}{dx}\right)^2 + \left(\frac{dA}{dy}\right)^2} \tag{5}$$

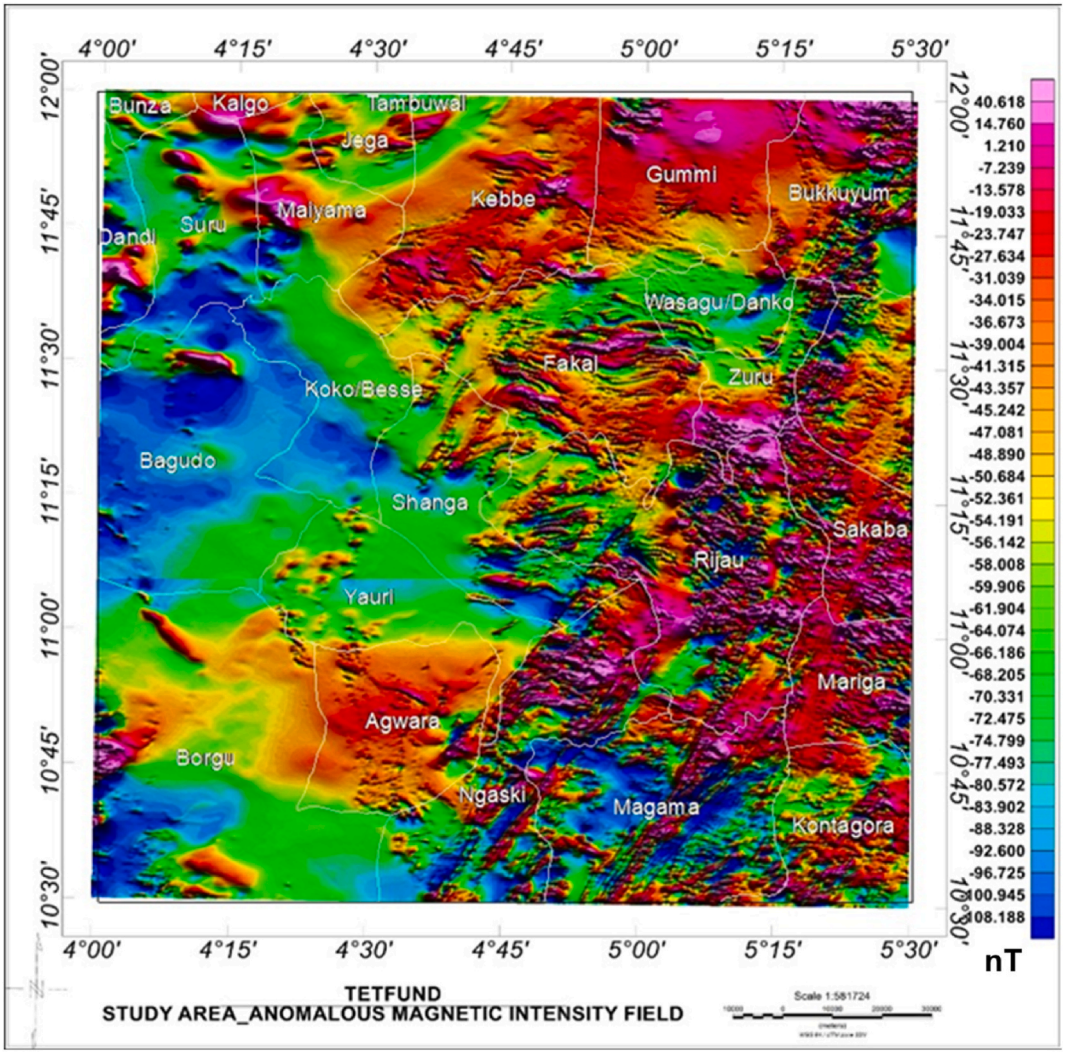

Fig. 2. Total magnetic intensity anomalous (TMIA) map of the study area.

where A is tilt derivative (Smith et al., 1998).

2.2.7. *Hydrothermal alteration indicators*

Hydrothermal alteration that hosts orogenic gold, usually occur within tectonically deformed crustal rocks that provide conduits hydrothermal fluids at a temperate range of 100–500 °C [31]. It has been proven that a relationship exists between potassium enrichment, thorium depreciation and gold mineralization process [31,32]. For the afore-mention reason, regions of magnetic lineaments that coincide with regions of potassium enrichment observed on the radiometric data are mapped as area of hydrothermal altered zones.

Due to the fact that thorium is geochemically immobile when compared with potassium and uranium, it is used for normalisation of the radiometric data due to lithology variations that is caused by environmental weathering and lithology on K and eU concentration [38–40]. It can be observed that thorium deprivation occurs majorly with potassium accentuation during hydrothermal alteration processes. This hydrothermal alteration sync-mineralization subsystem is usually associated with volcanic-associated massive-sulfide (VMS) base-metal and gold deposits [31,41–43].

Efmov (1978) used cum deviation from ideal potassium values (K_d) to map hydrothermal alteration haloes associated with orogenic gold mineralization in the area of interest. These techniques have been modified to specifically mark out regions that have suffered potassium enrichment, the ratio of equivalent thorium concentration to the measured potassium counts (eTh/K); the F_parameter, defined by the ratio of the product of potassium (K) counts and equivalent uranium (eU) concentration to the equivalent of thorium (eTh) concentration.

The potassium Deviation (K_d) from the nominal K values which represent potassium enrichment values due to hydrothermal

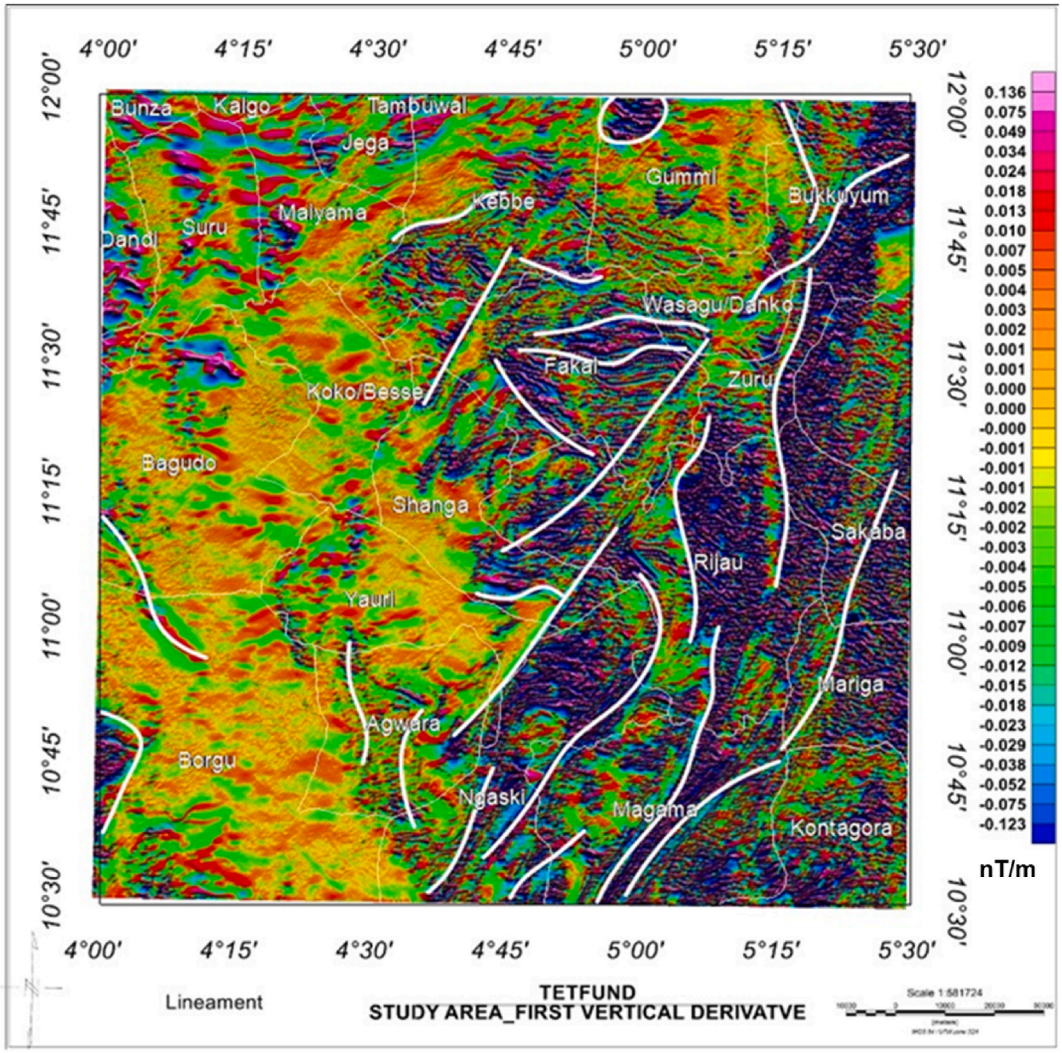

Fig. 3. Map of first vertical derivative (FVD) result of the study area.

alteration processes is obtained from Equation (6), de Quadros et al. (2003):

$$K_d = \left(\frac{K - K_n}{K_n}\right) \tag{6}$$

where K_d represents the potassium deviation, K is the measured field potassium concentration and K_n the nominal potassium value.

Employing the method develop by Refs. [39,40] the nominal K value (K_n) is obtain from the relation [32].

$$K_n = \left(\frac{K\,grid_{average}}{Th\,grid_{average}}\right) \times Th\,Map \tag{7}$$

Values of $K\,grid_{average}$ and $Th\,grid_{average}$ can be evaluated from the statistical tools on Oasis Montaj software, a high K_diviation value is an indication of hydrothermal alteration.

The F which reflects two relevant relationships, the richness of K related to eTh/eU ratio and the richness of eU related to the eTh/K ratio giving by equation (8) [32]:

$$F = \frac{K \times eU}{eTh} = \frac{K}{\frac{eTh}{eU}} = \frac{eU}{\frac{eTh}{K}} \tag{8}$$

The $\frac{eTh}{K}$ ratio is simply the incense of the $\frac{K}{eTh}$ earlier computed. The $\frac{eTh}{K}$ result will serve as to correlate the expected highs from F_parameter and K_deviation analysis hence its low regions should coincide with regions of high regions.

To have a holistic treatment to the results from the three approaches, the integration of these results can be archive by constructing

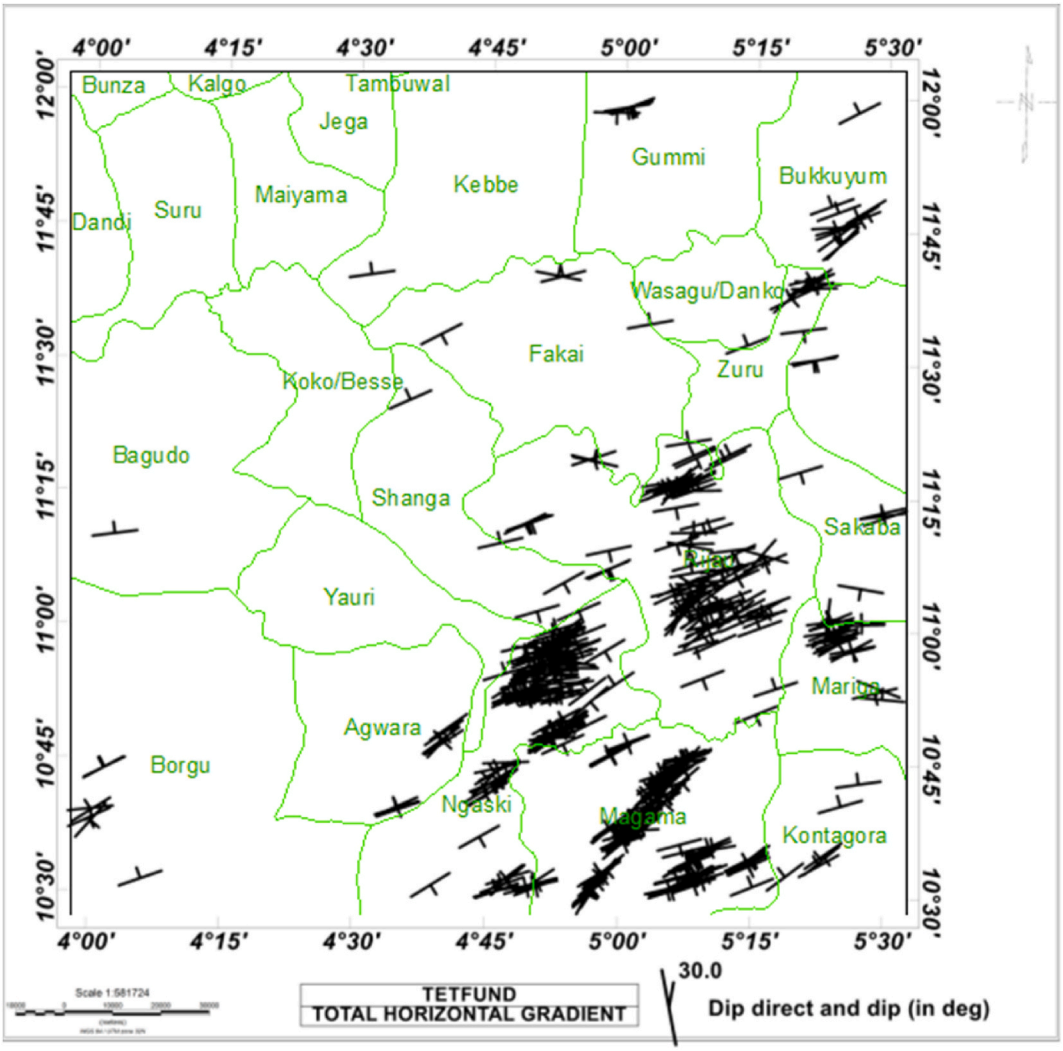

Fig. 4. Total horizontal gradient map of the study.

a ternary image, in RGB (Red for K_deviation, Green for F_parameter, and Blue for K/eTh). However, for an acceptable analysis, it is essential that the various analyses are trending in the same direction (i.e positive anomalies are correlating) [45].

3. Results and discussion

3.1. Airborne magnetic data results

The NGSA data was in gridded format, and each sheet presented on a scale of 1:100000, covering 55 × 55 square kilometers, these grids (sheets) were merged to produce a single grid (TMI). This was achieved using an appropriate extension on the Oasis Montaj of Geosoft software, and then mapped to obtain Fig. 1S, 2 and 2S, 3, 3S, 4, 5 and 6.

3.1.1. Total magnetic intensity (TMI) result

Fig. 2 shows a colour aggregate map representation of the TMI anomaly of the study area when IGRF (33,000 nT) was removed. The map gives the vector sum of all components of the magnetic field. It is primarily used in this study to reveal the magnetic characteristic of the various lithological units in the area. The magnetic signatures range from a low susceptibility of −108.188 nT (minimum) towards the western region of the study area, to a high magnetic susceptibility of 40.618 nT (maximum) at the southern parts of the region.

The regions with high magnetic signatures (−39.004 nT–40.618 nT) indicated in red/pink, were Kebbe, Gummi, Bukkuyum, Sakaba, Zuru, Rijau, Mariga, Kontagora, Agwara, and the northeastern part of Ngaski. Low magnetic signature (−108.188 nT to −54.919 nT) regions which are signified with blue/green colour included the Bagudo, Koko/Besse, Shanga, Suru, Maiyama, Jega,

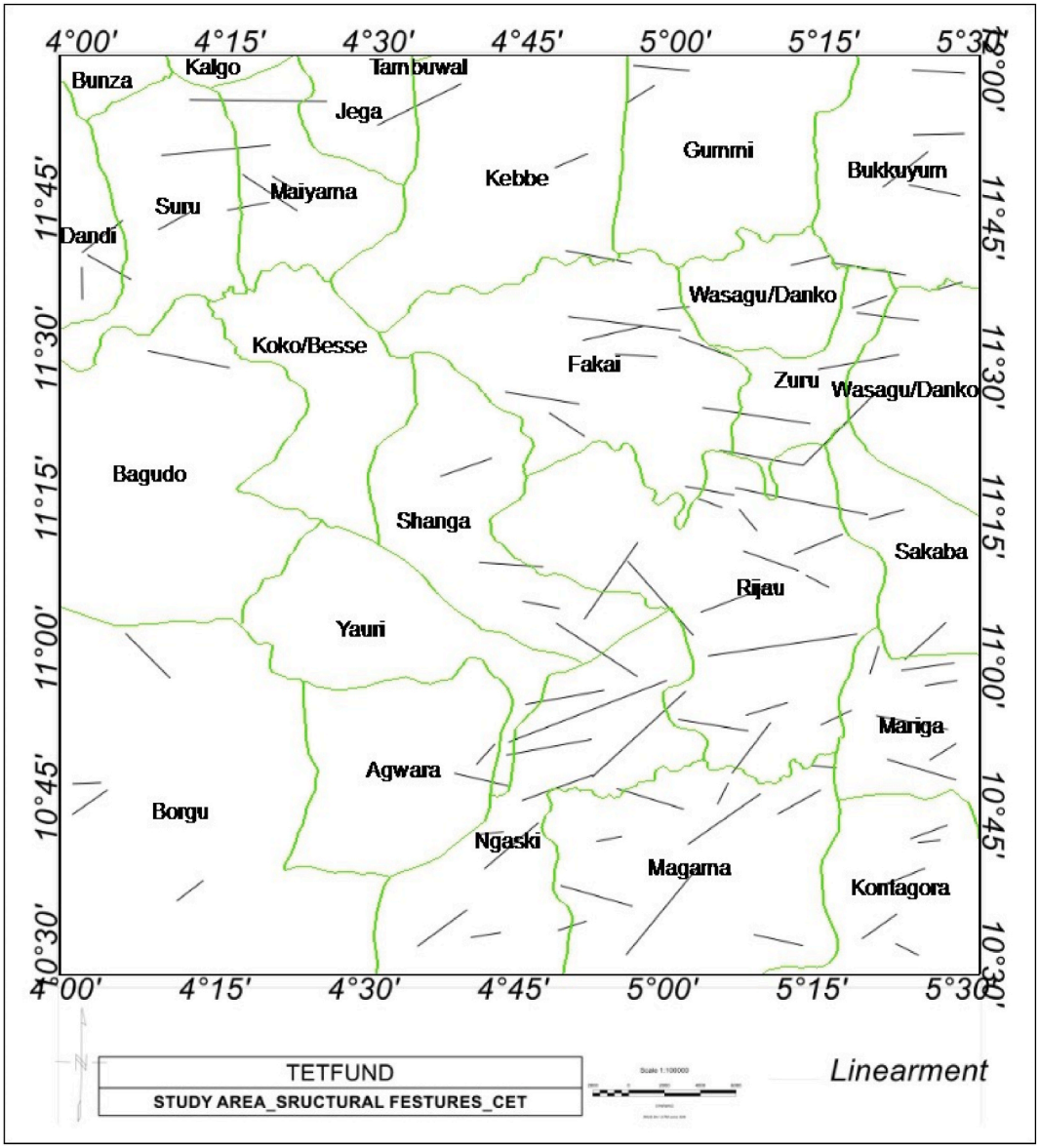

Fig. 5. Centre for exploration targeting (CET) map of the study area.

Wasagu/Danko, and Borgu. Thus, low and high regions are distinguished by different rock formations that result in variations in the magnetic susceptibility of the rocks within the area. The susceptible rocks typically occur at depths shallower than the Curie point isotherm [46].

3.1.2. First vertical derivative (FVD) result

The FVD map (Fig. 3) aids in the attenuation of long-wavelength magnetic anomalies within the field, which is important in improving closely spaced resolution and superimposed anomalies, which were previously not visible in TMIA map (Fig. 2). Fig. 3 exhibits some regular linear structures that could be regarded as lineaments that infer fractures, faults, and joints. Lineaments, which might be fractures, faults, or shear zones, are typically used as channels for mineral deposits. These structures are the features that control the mineralization pattern of the study area [46]. The following locations were identified as major structural zones of interest: the SE parts of Yauri and Shanga, Fakai, Ngaski, Zuru, Magama, Rijau, the eastern half of Wasagu/Danko, and Bukkuyum. These structures trends majorly in NE-SW, few others in NW-SE and E-W.

3.1.3. Total gradient amplitude (TGA) result

The obtained TGA map (Fig. 1S), enhanced the visualisation of the variation of the magnetization of the magnetic sources across the

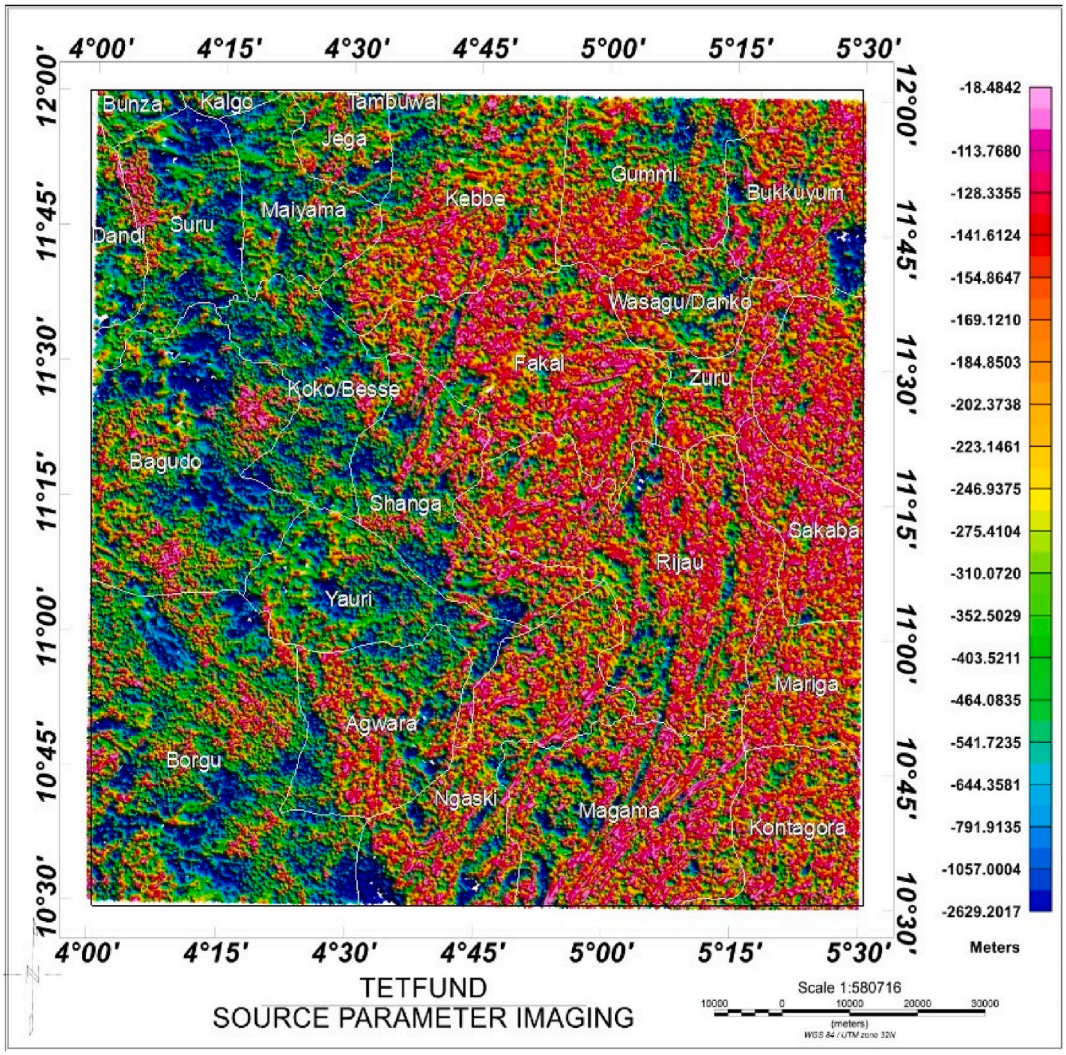

Fig. 6. Source parameter imaging (SPI) map of the study area.

field and also indicates the boundaries of anomaly texture. This filter enhances near surface basement. Looking at the map closely, across the field over the edge of the magnetic associated with the presence of ferromagnetic, Fe bearing rocks with some felsic minerals as revealed on the geological setting of the area. The map displayed two different magnetic zones with difference colour aggregates. These zones are: low, in a green colour (0.034–0.050 nT/m) and high, in red/pink colour (0.056–0.226 nT/m).

Low magnetic susceptibility, shown in blue (Fig. 1S), has low amplitudes ranging from 0.034 to 0.050 nT/m which corresponded to: Bagudo, Koko/Besse, Suru, Shanga, the northern part of Zuru, Yauri, the southern part of Ngaski, Wasagu/Danko, the northern part of Borgu and Magama. These zones were associated with sandstones, siltstones, clay shales, limestone and laterites as compared with the geology of the area. The sediments within these zones may be strongly controlled by the carbonate content of the depositional environment and also the carbonates species are usually strongly dependent on both sedimentary facies and sediment provenance [46].

However, the zones with the highest amplitude marked in red/pink (0.056–0.226 nT/m) are the regions associated with; granite, rhyolite, biotite-granite, meta-conglomerate, quartz-mica schist, migmatite and gneiss as compared with the geological setting of the area. These regions also fall under the following areas Shanga, Yauri, Ngaski, Zuru, Fakai, Wasagu/Danko and Sakaba areas of Kebbi State, Kebbe and Bukkuyum areas of Zamfara State and, Rijau, Magama and Mariga areas of Niger State. When compared with the zones of highest amplitudes (0.056–0.226 nT/m) in relation to susceptibility of common rocks, it can be noticed that the locations have significant positive magnetic susceptibility values, which correspond to the presence of ferromagnetic materials such as gold. These areas with ferromagnetic properties may usually contain mafic and ultramafic that host more Fe-bearing minerals (gold mineral) [46]. The type of rock formations highlighted in these zones may contribute significantly to identifying the species of crystallised gold with the increase of the oxidised Fe-bearing minerals from mafic to felsic rocks.

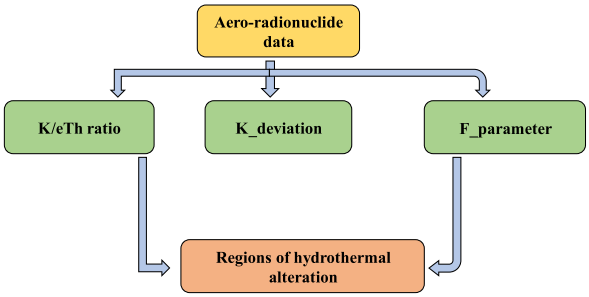

Fig. 7. Work flow chart for hydrothermal alteration.

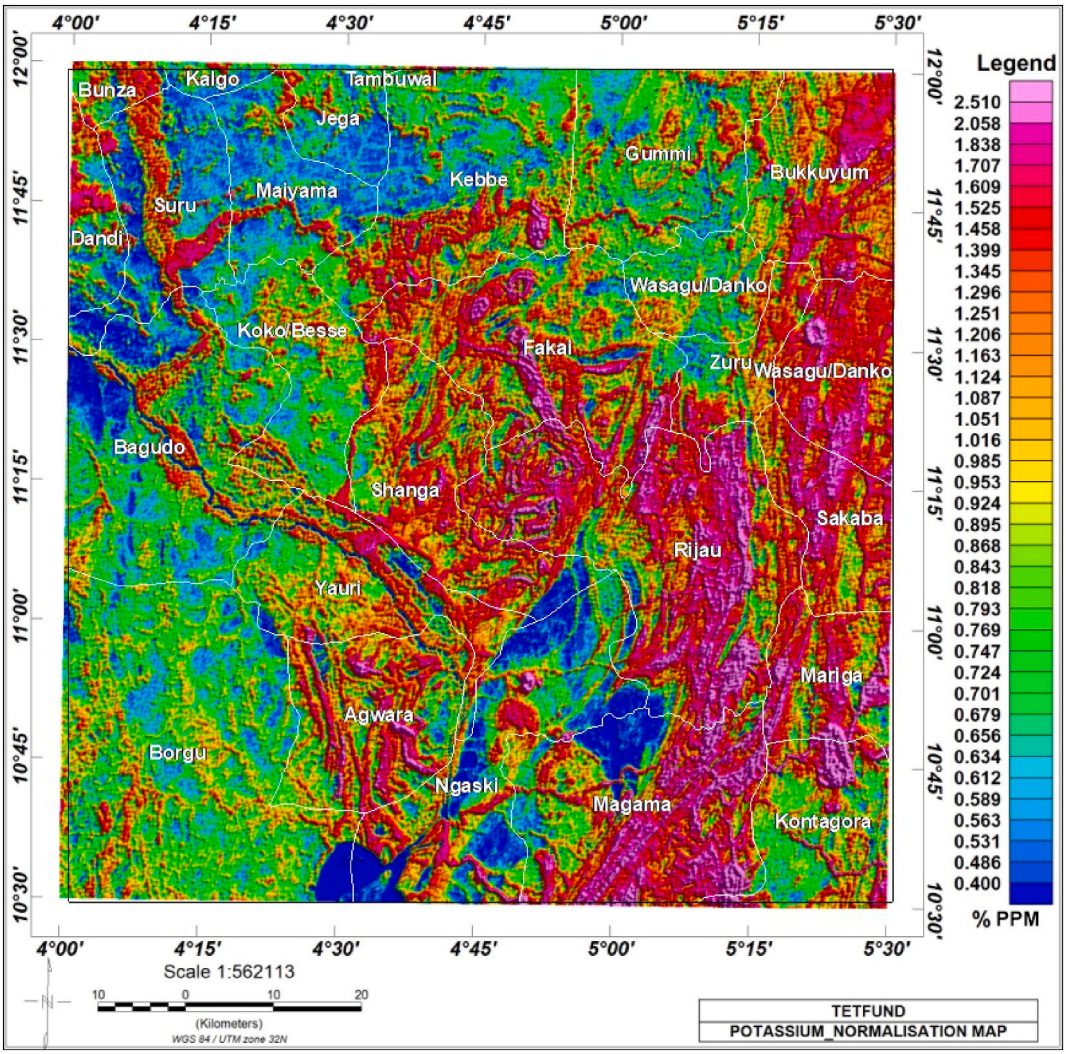

Fig. 8. Potassium normalisation map.

3.1.4. Total horizontal derivative (THD) result

Fig. 2S shows the THD map of the area generated from TMI anomalies using magnetic data. The map reveals the horizontal location and extent of the edges of various magnetic sources. The edges of the shallow and deep sources of magnetic anomalies were more pronounced in the south-eastern part of the study area. These regions are located at the SE parts of Yauri and Shanga, Fakai, Ngaski, Zuru, Magama, Rijau, Wasagu/Danko, and Bukkuyum. The structures revealed the spatial location of the magnetic source edges. When compared to the geological setting of the area, the regions were underlying by Granite, rhyolite, biotite-granite, meta-conglomerate,

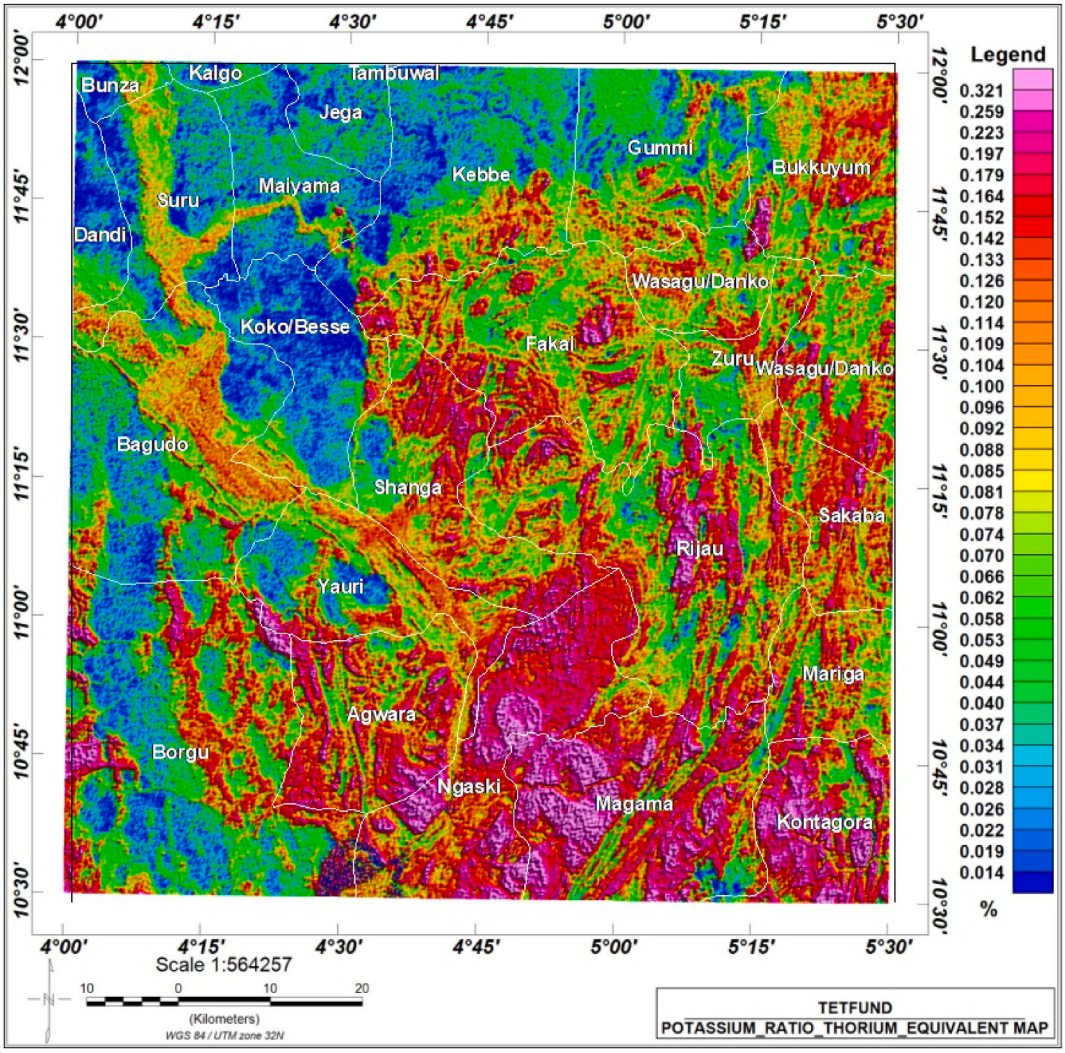

Fig. 9. Potassium_ratio_Thorium map.

quartz-mica schist, migmatite, and gneiss. These structures could play a role in determining the presence of minerals.

3.1.5. Source edge detection (SED) result

The source edge detection (SED) filter is achieved by employing the result from the total horizontal derivative (THD) as input, it locates peaks from the THD data. In general, peaks observed on the SED filter align with the corresponding edges of magnetic sources, which in turn defines the geological contacts within an investigated area. The strike of the magnetic field anomalies is displayed in a feathery-like symbol.

Fig. 4 depicts the horizontal location and extent of the edges of various magnetic sources. The edges of the magnetic anomaly sources were more apparent in the southeastern section of the research area. These areas are in the SE portions of Yauri and Shanga, Fakai, Ngaski, Zuru, Magama, Rijau, Wasagu/Danko, and Bukkuyum. The structures showed the spatial location of the magnetic source edges. When contrasted with the geological background of the area, the regions were underlain by granite, rhyolite, biotite-granite, meta-conglomerate, quartz-mica schist, migmatite, and gneiss. These structures may play a role in determining the existence of minerals, particularly gold mineralization.

3.1.6. Center for exploration targeting (CET) result

The technique began with the Texture Analysis Standard Deviation, which offers an estimate of the local variations in the data at every position in the grid. This method computes the standard deviation of the data values within the immediate neighbourhood.

The next step was the usage of the Phase Symmetry and Phase Congruency of Lineation Detection, which is different from traditional gradient-based edge detection algorithms. It is beneficial for locating step edges, which are the boundaries of most magnetic anomalies that do not have identifiable step edges but instead change bands smoothly. According to Ref. [17], the phase congruency

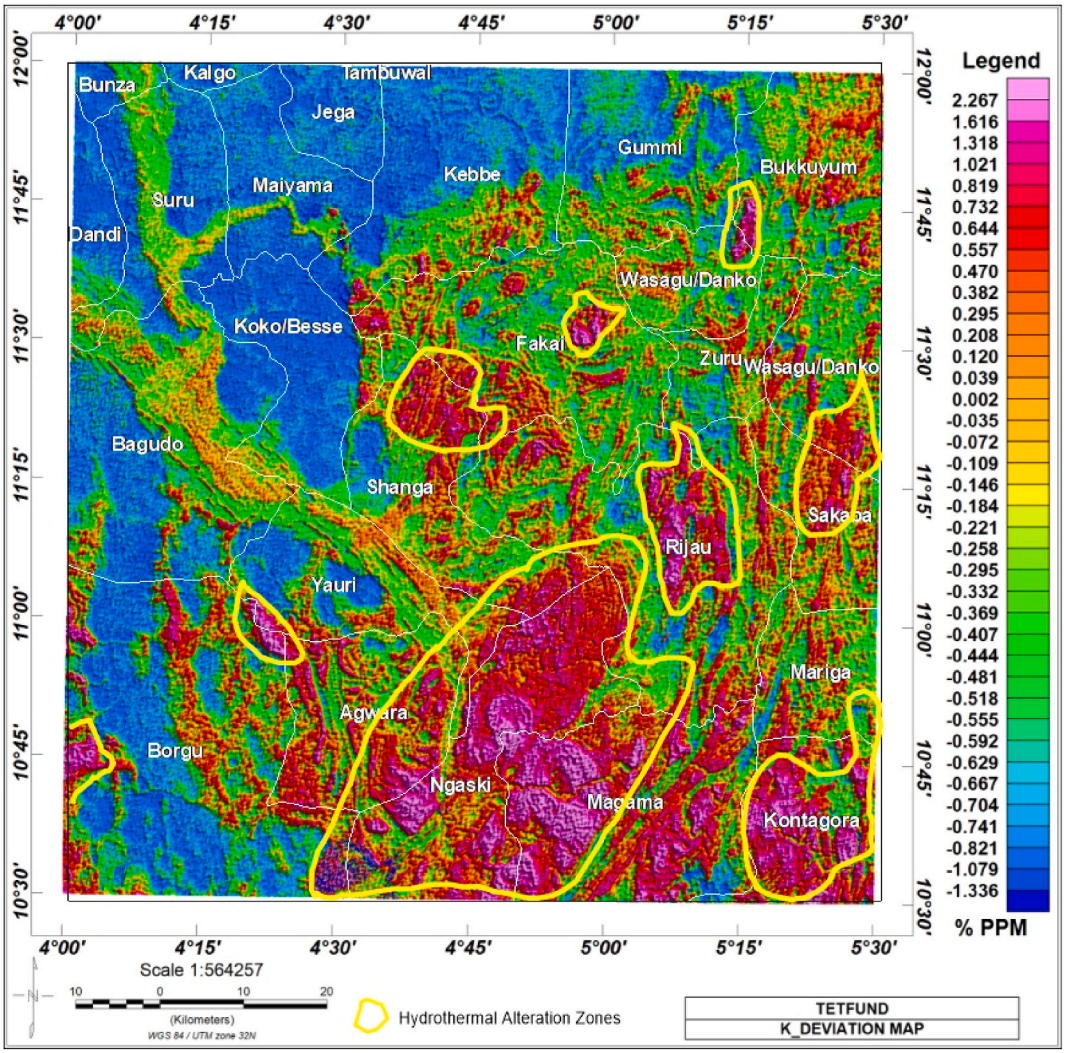

Fig. 10. Potassium_deviation map.

transform, like the phase symmetry transform, is a contrast-invariant edge detection method based on detecting the local spatial frequencies. It takes advantage of the fact that edge characteristics appear at sites when the local frequency components are most in phase.

The result of the procedures is transferred through Amplitude Thresholding in conjunction with non-maximal suppression (NMS). It takes into account the local feature orientation to maximize feature continuity and can be used to eliminate noise and highlight linear features.

Lastly, Skeleton to Vectors is then used. The Skeleton to Vectors plug-in uses a line fitting method to vectorise the skeletonised structures created by the Skeletonisation plug-in. Vectorised data from these processes was subsequently utilised as input to structural complexity map plug-ins. This procedure is repeated iteratively until no structure segment deviates more than the specified tolerance from its associated line segment. The vectorised representation of the structures within the grid is formed by these line segments [17].

The obtained CET map (Fig. 5) reveals the linear structures (lineament) within the South-East of the study area which corresponds to; SE parts of Yauri and Shanga, Fakai, Ngaski, Zuru, Magama, Rijau, Eastern part of Wasagu/Danko and Bukkuyum. These structures were located within the basement regions of the area and were correlated well with the geology of the area. From Fig. 5, it can be observed that most of the linear structures trend in the NE-SW directions which delineate faults, fractures/or shears zones that represent surface structural features of possible gold mineralized zones.

Geologically (Fig. 1), these regions fall under the following rock types; quartz-mica schist, Migmatite, Granite, Biotite, Gneiss and Diorite. Because the majority of gold deposits in Nigeria are found in quartz veins, the rocks discovered inside the structural trend of alteration zones play a significant role in determining the gold mineral. The CET (Fig. 4) result agrees well with the structures in Figs. 3 and 4.

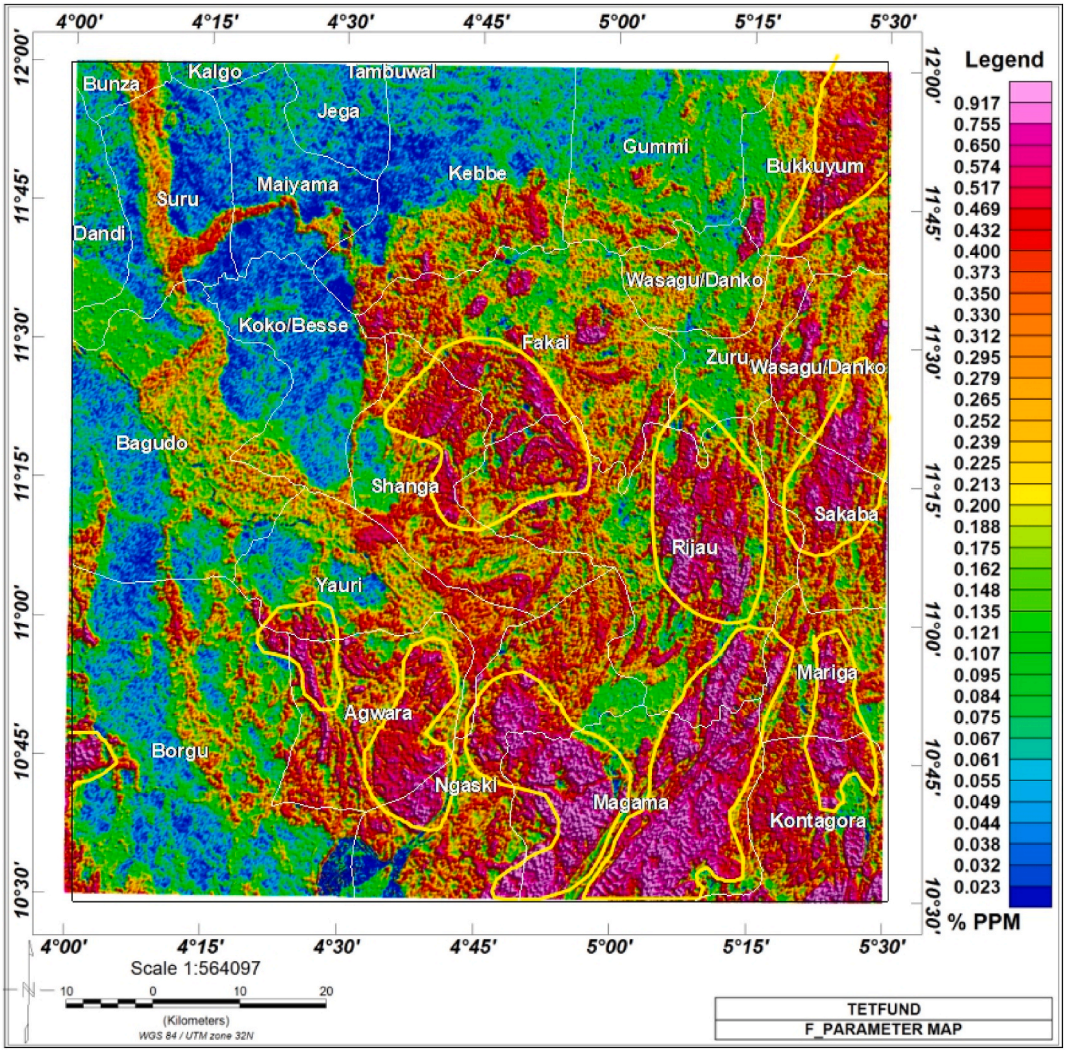

Fig. 11. F_parameter map.

3.1.7. *Euler Deconvolution (ED) result*

Fig. 3S show Euler deconvolution for faults/structures. The map depicts the Euler depths of the structures/faults that could host gold mineralization. The connectivity of these structures are defined at depths below 5 m. These findings revealed shallow depths in the areas corresponding to Fakai, the SE parts of Yauri and Shanga, Ngaski, Zuru, Magama, the eastern part of Wasagu/Danko, and Bukkuyum. These areas are part of the Nigerian basement complex, which usually controls mineralization based on the 1VD, TGA, TDR, and CET results as well as the geological setting of the area (Fig. 1). The deeper depth regions on the Euler depth map ranged from 10 m and above in Bunza, Bagudo, Dandi, Jega, Suru, Koko/Besse, western parts of Yauri and Shanga, and southern parts of Borgu.

3.1.8. *Source parameter imaging (SPI) result*

The SPI technique often delivers an average depth of the magnetic source and it is incapable of adequately mapping the undulating basement. The SPI results reflect the depth/thickness of the sediments that spanned the sedimentary basin and basement complex zones.

Fig. 6 revealed the depth to magnetic sources as well as the depth to basement rock contact, fractures, or faults with dykes. Looking closely at the map, the depths were separated into two categories: 223.1461 m–2629.2017 m, which is blue/green in colour, and below 18.4842 m, which is pink in colour. The obtained SPI depth map aided in specifying the depth of the causative body boundaries and trends of structures shown in Fig. 6. The pink-colour zones below 18.4842 m depth correspond to fault/structural trend regions (see Figure of 1VD), identified in the SE parts of Yauri and Shanga, Fakai, Ngaski, Zuru, Magama, Rijau, the eastern part of Wasagu/Danko, and Bukkuyum. While regions with blue to green colours reveal the zones of the sediments that crossed the areas of the sedimentary basin. The depth to the magnetics source of sedimentary regions was found to be from 223.1461 to 2629.2017 m. These areas were located in the following areas: Bunza, Kalgo, Tambuwal, Dandi, Suru, Bagudu, Koko/Besse, Borgu, Western parts of Shanga and Yauri.

Table 1
Integrated hydrothermal alteration zones from the K/Th ratio, K-deviation and F-parameter.

S/No	Summarized integrated results of K/Th ratio, K-deviation and F-parameter		
	Coordinate	Geological setting of the zones	Location
1	5°21′9″E, 10°40′12.72″N to 5°31′40.08″E, 10°40′28.2″N, and 5°32′3.12″E, 10°28′1.92″N to 5°20′38.4″E, 10°28′17.04″N	Diorite and migmatite, quartz-mica schist, medium coarse-grained, biotite-hornblende granite and biotite gneiss	Northern part of Kontagora
2	5°1′16.68″E, 11°15′5.4″N to 5°9′13.68″E, 11°13′56.28″N, and 5°8′50.28″E, 11°1′53.04″N to 5°1′54.84″E, 11°1′22.08″N	Quartz-Mica schist, Diorite and Migmatite	Western part Rijau
3	5°26′39.84″E, 11°23′33″N to 5°31′55.2″E, 11°24′42.48″N, and 5°32′10.68″E, 11°12′31.68″N to 5°28′35.4″E, 11°14′3.84″N.	Diorite, Migmatite, and Biotite Gneiss	NW part of Sakaba
4	4°37′10.2″E, 11°28′10.2″N to 4°44′44.16″E, 11°29′50.28″N, and 4°47′48.84″E, 11°20′5.28″N to 4°38′3.84″E, 11°19′50.16″N	Migmatite, Granite, Biotite Gneiss, Diorite, Sandstones, Ironstones and Laterites	NE part of Shanga
5	4°13′19.2″E, 11°0′5.4″N to 4°15′6.84″E, 11°1′6.96″N, and 4°18′34.56″E, 10°56′37.68″N to 4°16′23.88″E, 10°55′59.16″N.	Undifferentiated Schist, including some Gneiss, Quartz-Mica schist, Diorite and Migmatite	NW parts of Yauri and NE part of Borgu
6	3°58′34.32″E, 10°46′22.08″N to 4°1′8.04″E, 10°46′37.56″N, and 4°0′52.92″E, 10°43′1.92″N to3°58′41.88″E, 10°42′23.4″N	Medium Coarse-grained, Biotite-hornblende Granite, Biotite Gneiss, Diorite, Migmatite and Undifferentiated Schist, including some Gneiss	NW part of Borgu
7	4°59′15.72″E, 11°38′0.6″N to 5°3′59.4″E, 11°37′11.64″N, and 5°2′38.4″E, 11°34′21.36″N to 4°59′15.72″E, 11°33′48.96″N	Quartz-Mica schist	NE part of Fakai
8	5°18′12.24″E, 11°54′4.32″N to 5°20′53.52″E, 11°53′45.6″N to 5°20′53.52″E, 11°45′44.28″N to 5°17′25.8″E, 11°45′44.28″N	Quartz-Mica schist, Medium Coarse-grained and Biotite-hornblende Granite.	Western part of Bukkuyum and Southern part of Gummi.

3.2. Airborne aero-radiometric data results

3.2.1. Potassium concentration

Potassium is readily present in igneous rocks that are the major lithology across the field. This is evident in its abundance in Fig. 4S, where its maximum concentration is notice, major at the North-eastern end, where medium grain granite porphyritic granite and granite gneiss are the in-situ rocks. Other particles of high concentration occur at middle portion of the study area down to the south-eastern corner, specifically around Rijau, Magama, Ngaski, Sakaba and Western Borgu. Relatively low concentration is evident at the Northwest and Southwestern end, these are areas occupied by various grades of schist. The northwestern corner of the study area equally indicatea low concentration on area of Cretaceous Sokoto sandstone.

3.2.2. Thorium concentration

The Thorium concentration in the study area varies from 4 to 25.1 ppm with maximum concentration at the Eastern flank of the area, Fig. 5S. Other regions of anomalous concentration can be seen at the mid region, but worthy of note is the very low concentration at the southern end and the North-western corner, down to the South west.

3.2.3. Uranium concentration

Fig. 6S illustrates the concentration of Uranium within the area which shows similar feature with Potassium concentration when compared with thorium concentration, though its concentration varies from 0.8 to 6.8 ppm highest at the North-Eastern corner, with maximum concentration are observed around Rijau, Magama, Ngaski, Sakaba and Agwara Though the low concentration within Borgu, Maiyama Kontagora and Bagudo.

3.2.4. Hydrothermal alteration

The Aero Radionuclide data of the study area was employed primarily to delineate region of hydrothermal alteration. This was achieved through the following procedural stages (Fig. 7).

1. Computing the K/eTh ratio, a high value of K/eTh concentration is an indicator to altered zones.
2. Potassium-deviation (K_deviation) is obtained from equation (6), a high value is an indicator of an hydrothermal altered zone
3. Computing the F-parameter using equation (8), equally, a high value of F_parameter indicated that the regions have suffered hydrothermal alteration.

Finally, a ternary image using the eTh/K ratio grid, K-deviation grid, and the F-parameter grid is produced for analysis of the regions of hydrothermal alteration.

Comparing the concentration of the elements Potassium, Thorium and Uranium maps with the normalized ratio maps of K/Th, U/Th and K concentration (Fig. 8), by the use of Thorium to normalise attenuation effect caused by lithology variations as a result of

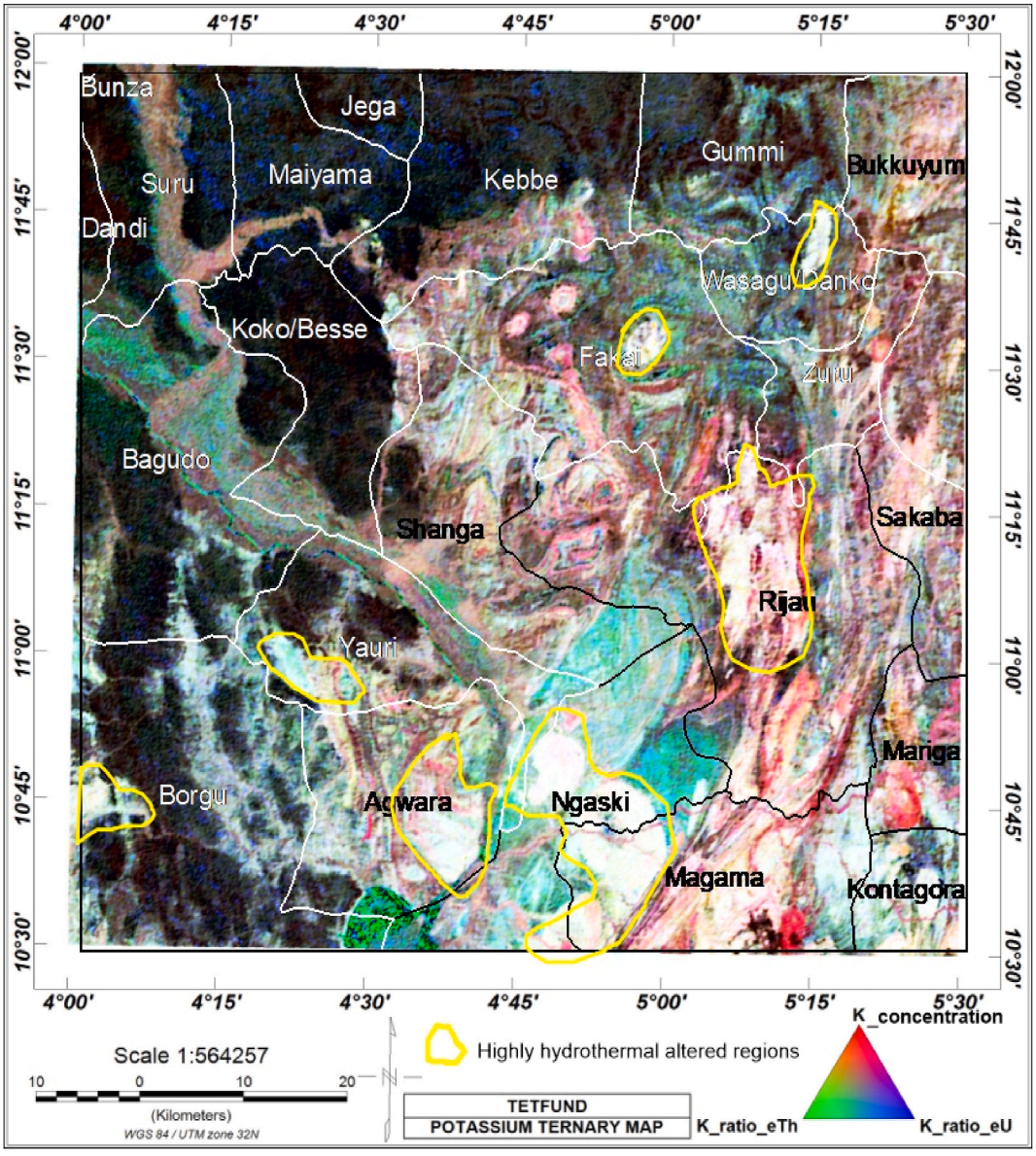

Fig. 12. Potassium_ternary map from potassium concentration, potassium_ratio_thorium and potassium_ratio_uranium grids map.

vegetation, water bodies and other contrasting literal lithological variations. This is clearly illustrated on the K/Th map Fig. 9. The intended aim of rationalising is clearly seen on the K/Th ratio map, Fig. 9. The highest anomalous region has shifted to the North-Western region and the North-Eastern regions where mainly rocks of Felsic igneous origin dominate. The regional highly low concentration at the middle of the map has been attenuated as patches of intermediate to high concentration intruding to the region that was initially deeply low.

As eTh is mobile compared to U and K, it is utilised as a lithological background control that defines ideal K value and concentration of eU in identification of hydrothermal altered halves. Thus, eTh values are needed to conquer effect of lithology on K and eU concentration (Saunders et al., 1987). Felsic rocks are light, composed of light colour minerals rich in silica content, poor in magnesium. Mafic rocks are dark in colour, rich in magnesium, and poor in silica.

The South-Eastern corners of the study area that host the Bida sandstone with medium concentration on the K concentration map are converted to low concentration on the K/Th ratio map. Similar observations were observed on the K/U ratio map, where the deep seated low K concentration has been normalized.

3.2.5. K-deviation, Th/K ratio and F-parameter maps

The potassium_ratio-Thorium map Fig. 9 was obtained for K/eTh grids, K_deviation map Fig. 10 (from equation (3)) and

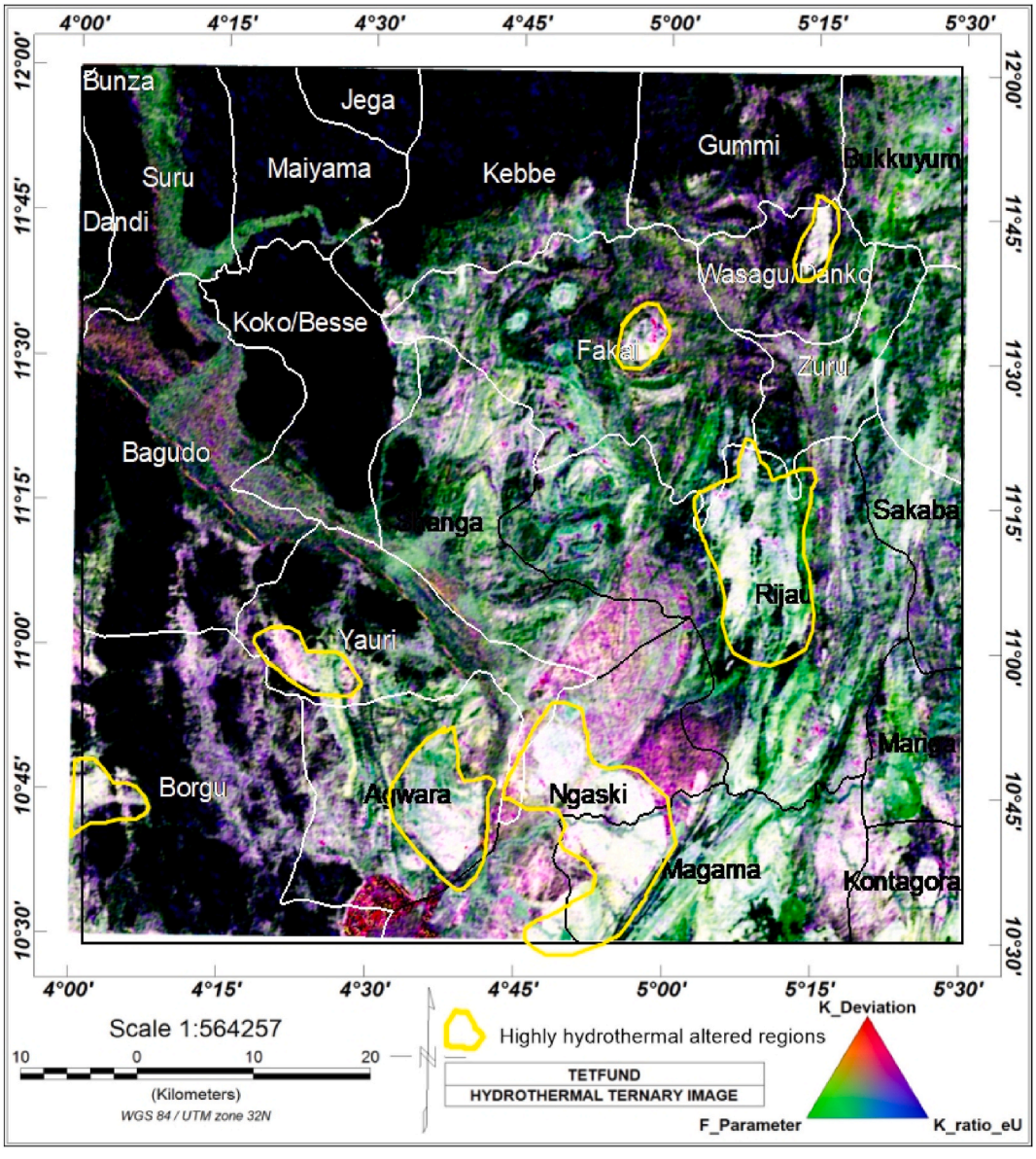

Fig. 13. Hydrothermal_Ternary map from potassium_deviation, potassium_ratio_thorium and parameter grids map.

F_parameter map Fig. 11 (from equation (5)) respectively these three results are the required information to targeted regions of hydrothermal alteration. Targets are anomalous high K-deviation and F-parameter coinciding with anomalous high K/Th that falls within regions of identified magnetic structures are the signatures that characterised regions of orogenic gold deposits [40–42]. The summarized results of these parameters given in Table 1 below.

3.2.6. Ternary image

The first ternary image, Fig. 12, was produced to indicate regions of potassium enrichment this was achieved by combining the measured Potassium concentration (as red) Potassium_ratio_Thorium (as Green) and Potassium_ratio_Uranium (as blue). Regions of anomalous response are depicted as white colour on the ternary map. The second ternary map was constructed to showcase Hydrothermal altered zones, this is achieved through the combination of the results from the three analysis viz, K/Th (B), K-derivative (R) and F-parameter (G) as shown in Fig. 13, area of anomalous high hydrothermal altered holes in white colour and moderate altered hydrothermal holes in (grey-blue) colour.

The ternary maps Figs. 14 and 15 represents the superposition of both the structural lineaments and fractures from FVD and CET respectively on the analysis of the radiometric data (hydrothermal zones), which interprets the faults zones, the rock type and location of hydrothermal alteration that are possible location of haloes of orogenic gold mineralization. Regions occupied by sandstone appears

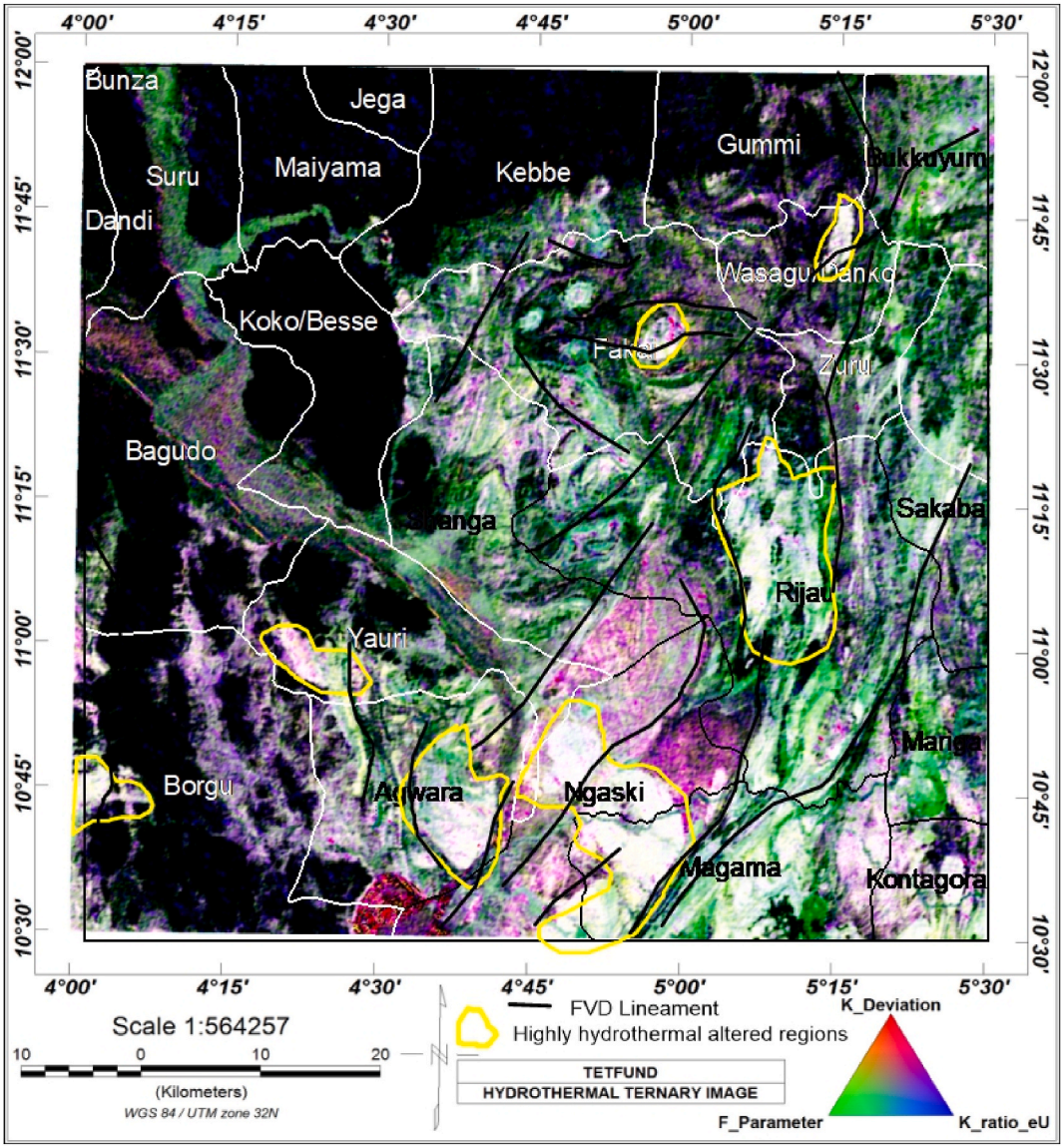

Fig. 14. Hydrothermal_ternary map superimposed on first vertical derivative lineament map.

black, indicating the result of low concentration of potassium within the Amphibolite Schists. The following are hydrothermal regions on ternary images falls within the coordinates and locations as given in Table 2 below.

4. Conclusion

Lineaments with gold mineralization attributes in Southern Parts of Kebbi State and its Environs, Northwestern Nigeria have been identified using the RTE, 1VD, TGA, TDR, SED and CET techniques. The directions of these major structures/or lineament were trending in the NE to SW directions. These structures were located within the basement regions of the area and were correlated well with the geology of the area. Most of these structures were delineated within zones of the south-eastern and north-eastern parts of the study area. The depth to the magnetic source's structures that could host gold mineralization was found to be less than 5 m using algorithm ED and SPI techniques. The resultant SPI depth, which aided in specifying the depth of the causative body boundaries and trends of structures, as well as the depth to the magnetics source of sedimentary regions, was found to be between 223.1461 and 2629.2017 m.

The radiometric data was normalized using a thorium grid due to its immobility, and the resulting normalized grids were used to obtain K/Th, K_deviation, and F_parameter analysis; a combination of these three produces a ternary image by combining K/Th, K-derivative, and F-parameter, which shows the area of anomalous high and moderate hydrothermal altered holes. The identified

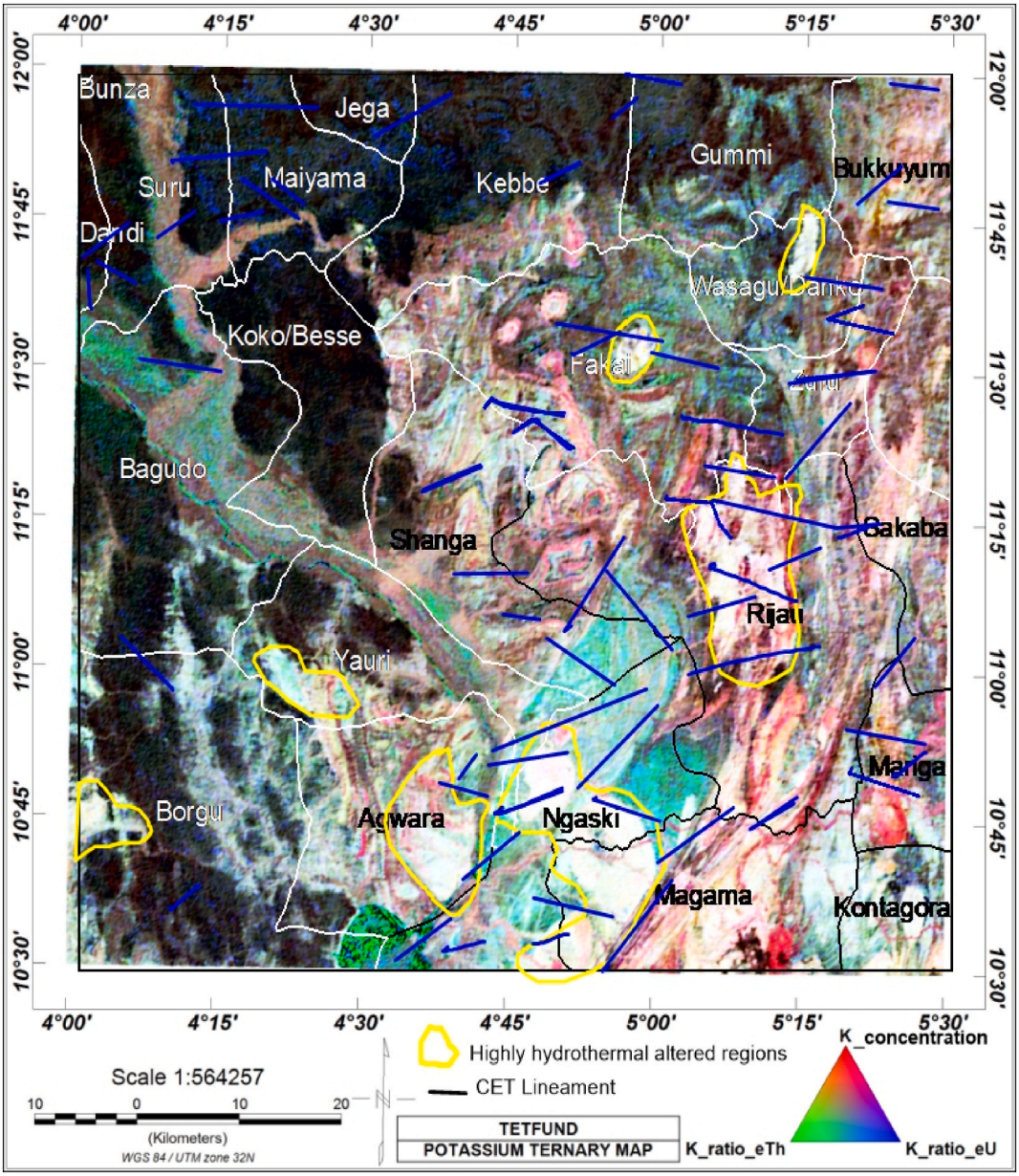

Fig. 15. Hydrothermal_ternary map superimposed on centre for exploration targeting (CET) lineament map.

hydrothermal regions of gold fields on ternary images, as well as zones of major structures, are located at Agwara, Western Magama, Rijau, Fakai, Bukkuyum, and Borgu in the south-eastern part of the study area with intrusive Quartz-Mica schist, Diorite, and Migmatite into the Granitic basement rocks. Delineation of the region as gold field is informed by major fault lines as observed on the first vertical derivative map, series of bristle fractures from the CET analysis, high value of K_deviation and F_parameter all these are clearly indicated on the two Ternary maps. The airborne magnetic and radiometric data processing techniques used in this study yielded a database containing precise coordinates, locations, and geological settings for potential gold mineralized zones. This database has been itemized in the subsections "K-deviation, Th/K ratio, and F-parameter maps" and "Ternary image," and these data could prove useful in the exploration of gold minerals in the area.

Data availability statement

The acquired datasets used in the current study are not available to the general public because the aeromagnetic and aeroradiometric data are under the custody of the Nigeria Geological Survey Agency (NGSA) and can only be released upon request and payment via their website (https://ngsa.gov.ng).

Table 2
Integrated hydrothermal alteration regions on Ternary images.

S/No	Summarized integrated results of K/Th ratio, K-deviation and F-parameter		
	Coordinate	Geological setting of the zones	Location
1	4°34′40.08″E, 10°50′18.24″N to 4°41′41.64″E, 10°48′49.32″N, and 4°39′48.24″E, 10°40′50.88″N to 4°33′35.28″E, 10°41′23.28″N	Quartz-Mica schist, Diorite and Migmatite	Eastern part of Agwara
2	4°45′36.72″E, 10°54′5.4″N to 5°3′59.4″E, 10°52′19.92″N, and 4°48′27″E, 10°30′2.16″N to 4°37′30.36″E, 10°30′18.36″N	Quartz-Mica schist, Medium Coarse-grained, Biotite-hornblende Granite, Diorite, Migmatite and Biotite Gneiss.	Western Magama
3	5°1′49.8″E, 11°16′55.56″N to 5°10′4.44″E, 11°15′58.68″N, and 5°9′7.56″E, 11°3′41.04″N to 5°1′41.52″E, 11°3′41.04″N.	Quartz-Mica schist, Medium Coarse-grained, Biotite-hornblende Granite, Diorite and Migmatite	NW part of Rijau
4	4°57′30.24″E, 11°35′50.64″N to 5°1′49.8″E, 11°34′54.12″N, and 5°1′17.4″E, 11°31′47.64″N to 4°57′38.52″E, 11°32′11.76″N	Quartz-Mica schist	NW part of Fakai.
5	5°14′56.04″E, 11°50′9.96″N to 5°18′27″E, 11°50′34.44″N, and 5°18′10.8″E, 11°45′2.16″N to 5°15′20.52″E, 11°44′5.28″N.	Quartz-Mica schist	SE part of Bukkuyum and Northern part of Wasagu/Danko
6	3°58′34.32″E, 10°46′22.08″N to 4°1′8.04″E, 10°46′37.56″N, and 4°0′52.92″E, 10°43′1.92″N to3°58′41.88″E, 10°42′23.4″N	Medium Coarse-grained, Biotite-hornblende Granite, Biotite Gneiss, Diorite, Migmatite and Undifferentiated Schist, including some Gneiss	NW part of Borgu.

CRediT authorship contribution statement

K.A. Salako: Writing – original draft, Methodology, Funding acquisition, Data curation, Conceptualization, Investigation, Validation, Visualization, Writing – review & editing. **A.A. Adetona:** Validation, Software, Conceptualization, Data curation, Investigation, Methodology, Writing – original draft, Writing – review & editing. **A.A. Rafiu:** Visualization, Conceptualization, Data curation, Investigation, Methodology, Supervision, Validation, Writing – original draft, Writing – review & editing. **A.I. Augie:** Writing – review & editing, Software, Conceptualization, Data curation, Formal analysis, Investigation, Methodology, Supervision, Validation, Visualization, Writing – original draft. **M.O. Jimoh:** Visualization, Conceptualization, Data curation, Funding acquisition, Investigation, Methodology, Software, Supervision, Validation, Writing – original draft, Writing – review & editing. **A. Alkali:** Writing – review & editing, Conceptualization, Data curation, Investigation, Methodology, Supervision, Validation, Visualization, Writing – original draft. **R.A. Muriana:** Writing – review & editing, Conceptualization, Data curation, Investigation, Methodology, Supervision, Validation, Visualization, Writing – original draft. **J.O. Lawrence:** Writing – review & editing, Conceptualization, Data curation, Investigation, Methodology, Supervision, Validation, Visualization, Writing – original draft.

Declaration of competing interest

No potential conflict of interest was reported by the author(s).

Appreciation/Acknowledgement

The research team appreciates the immense contribution of TETFund for full sponsorship of this research through her annual National Research Fund (NRF-Grant) intervention to Nigeria Tertiary Education.

Appendix A. Supplementary data

Supplementary data to this article can be found online at https://doi.org/10.1016/j.heliyon.2024.e34093.

References

[1] P.D. Maghfira, S.W. Niasari, Magnetic data analysis to determine the subsurface structures in candiumbul geothermal prospect area, central java, in: American Institute of Physics (AIP) Conference Proceedings, vol. 1861, 2017 030041, https://doi.org/10.1063/1.4990928.
[2] M. Adama, M. Abu, A.N. Naeem, 2D-Modeling of the major structures within the Chad basin, Nigeria, from aeromagnetic data, Int. J. Soc. Res. Methodol. 12 (4) (2019) 99–113.
[3] A.A. Adetona, K.A. Salako, A.A. Rafiu, Delineating the lineaments within the major structures around eastern part of Lower Benue Trough from 2009 aeromagnetic data, FUW Trends in Science & Technology Journal 3 (1) (2018) 175–179.
[4] J.S. Ejepu, C.I. Unuevho, T.A. Ako, S. Abdullahi, Integrated geosciences prospecting for gold mineralization in Kwakuti, north-central Nigeria, Journal of Geology and Mining 10 (7) (2018) 81–94, https://doi.org/10.5897/JGMR2018.0296.
[5] P. Kearey, M. Brooks, I. Hill, An Introduction to Geophysical Exploration, Blackwell Scientific Publications, New York, NY, 2002.
[6] M.A. Sani, J. Raimi, S.M. Elatikpo, K.M. Lawal, Magnetic interpretation of structures associated with gold mineralisation around Kundila and Ginzo area, northwestern Nigeria, Nigerian Journal of Scientific Research 16 (2) (2017) 240–246, njsr.abu.edu.ng.

[7] S.O. Elkhateeb, M.A.G. Abdellatif, Delineation potential gold mineralization zones in a part of Central Eastern Desert, Egypt using airborne magnetic and radiometric data, NRIAG Journal of Astronomy and Geophysic (2018), https://doi.org/10.1016/j.nrjag.2018.05.010.
[8] T. Hoschke, M. Sexton, Geophysical exploration for epithermal gold deposits at Pajingo, North Queensland, Australia, Explor. Geophys. 36 (2005) 401–406.
[9] H. Andrson, C. Nash, Integrated lithostructural mapping of the Rossing area, Namibia, using high-resolution aeromagnetic, aeroradiometric, Landsat data and aerial photographs, Explor. Geophys. 28 (1997) 185–191.
[10] A.A. Adetona, F.I. Kwaghhua, S.B. Aliyu, Interpreting the magnetic signatures and radiometric indicators within Kogi State, Nigeria for economic resources, Geosystems and Geoenvironment 2 (2022) 100157, https://doi.org/10.1016/j.geogeo.2022.100157, 2023.
[11] S.B. Aliyu, A.A. Adetona, A.A. Rafiu, J. Ejepu, T. Adewumi, Delineating and interpreting the gold veins within Bida and Zungeru Area, Niger State Nigeria, using aeromagnetic and radiometric data, Pakistan Journal of Geology (PJG) 5 (2) (2021), https://doi.org/10.2478/pjg-2021-0006. ISSN: 2521-2915.
[12] H.G. Miller, V. Singh, Potential field tilt-a new concept for location of potential field sources, J. Appl. Geophys. 32 (1994) 213–217.
[13] L. Cordell, V.J.S. Grauch, Mapping basement magnetization zones from aeromagnetic data in the San Juan Basin, New Mexico, in: W.J. Hinze (Ed.), The Utility of Regional Gravity and Magnetic Maps, Society of Exploration Geophysicists, 1985, pp. 181–197.
[14] M.O. Arisoy, U. Dikmen, Edge detection of magnetic sources using enhanced total horizontal derivative of the tilt angle, Bull Earth Sciences Applied Research Cent Hacet University 34 (1) (2013) 73–82.
[15] G.J. Cooper, D.R. Cowan, Edge enhancement of potential- field using normalized statistics, Geophysics 73 (3) (2008) H1–H4.
[16] F.F. Ferreira, L.G. de Castro, A.S. Bongiolo, J. de Souza, M.T. Romeiro, Enhancement of the Total Horizontal Gradient of Maznetic Anomalies Using Tilt Derivatives: Part II—Application to Real Data, SEG Technical Program Expanded Abstracts, 2011, pp. 887–891.
[17] P. Kovesi, A dimensionless measure of edge significance, in: Proc. DICTA-91, Melbourne, 1991, pp. 281–288.
[18] J. Macnae, Applications of geophysics for the detection and exploration of kimberlites and lamproites, in: W.L. Griffin (Ed.), Diamond Exploration into the 21st Century, Journal of Geochemical Exploration, 1995, pp. 213–243.
[19] D. Core, A. Buckingham, S. Belfield, Detailed structural analysis of magnetic data-done quickly and objectively, SGEG Newsletter 1 (2) (2009) 15–21.
[20] D.F. Graham, Airborne radiometric data a tool for reconnaissance geological mapping using a GIS Thematic Conference, in: Proceedings, 9th, Geologic Remote Sensing, vol. 1, 1993, pp. 43–54. Pasadena, CA, February 8–11, 1993.
[21] A.L. Jaques, P. Wellman, A. Whitaker, D. Wyborn, High-resolution geophysics in modern geological mapping, AGSO J. Aust. Geol. Geophys. 17 (1997) 159–173.
[22] B.W. Charbonneau, P.B. Holman, R.J. Hetu, Mac Queen, Airborne gamma spectrometer magnetic-VLF survey of northeastern alberta, exploring for minerals in alberta: geological survey of Canada geoscience contributions, geological survey of Canada bulletin, Canada-Alberta Agreement on Mineral Development 500 (1997) 107–132.
[23] T.M. Ramadan, M.F. AbdelFattah, Characterization of gold mineralization in Garin Hawal area, Kebbi State, NW Nigeria, using remote sensing, Egyptian Journal of Remote Sensing and Space Science 13 (2) (2010) 153–163, https://doi.org/10.1016/j.ejrs.2009.08.001.
[24] D.S. Bonde, S. Lawali, K.A. Salako, Structural mapping of solid mineral potential zones over southern part of Kebbi state, northwestern Nigeria, Journal of Scientific and Engineering Research 6 (7) (2019) 229–240.
[25] E.J. Holden, M. Dentith, P. Kavesi, Towards the automatic analysis of regional aeromagnetic data to identify regions prospective for gold deposits, Computer Geoscience 34 (2008) 1505–1513, https://doi.org/10.1016/j.cageo.2007.08.007.
[26] S. Lawali, K.A. Salako, D.S. Bonde, Delineation of mineral potential zones over lower part of Sokoto Basin, northwestern Nigeria using aeromagnetic data, Acad. Res. Int. 11 (2) (2020) 19–29.
[27] L.M. Adamu, N.G. Obaje, A.A. Sidi, A.K. Aweda, H.M. Liman, Geochemical evidence for the origin of the daranna manganese deposit, Kebbi state, Nigeria, Nigerian Journal of Basic and Applied Science 29 (2) (2021) 30–45, https://doi.org/10.4314/njbas.v29i2.4.
[28] M.M. Lawal, K.A. Salako, M. Abbas, T. Adewumi, A.I. Augie, M. Khita, Geophysical investigation of possible gold mineralisation potential zones using a combined airborne magnetic data of lower Sokoto Basin and its environs, northwestern Nigeria, International Journal of Progressive Sciences and Technologies (IJPSAT) 30 (1) (2021) 1–16.
[29] A.I. Augie, K.A. Salako, A.A. Rafiu, M.O. Jimoh, Geophysical assessment for gold mineralisation potential over the southern part of Kebbi State using aeromagnetic data, Geology, Geophysics & Environment 48 (2) (2022) 177–193, https://doi.org/10.7494/geol.2022.48.2.177.
[30] A.I. Augie, K.A. Salako, A.A. Rafiu, M.O. Jimoh, Geophysical magnetic data analyses of the geological structures with mineralisation potentials over the southern part of Kebbi, NW Nigeria, Min. Sci. 29 (2022) 179–203, https://doi.org/10.37190/msc222911.
[31] L.O. Cunha, A.C. Dutra, A.B. Costa, Use of radiogenic heat for demarcation of hydrothermal alteration zones in the Pernam- buco-Brazil, J. Appl. Geophys. 145 (2017) 111–123.
[32] T.P. de Quadros, J.C. Koppe, A.J. Strieder, J.L. Costa, Gamma- ray data processing and integration for lode-Au deposits exploration, Nat Resource Research 12 (1) (2003) 57–65.
[33] U.A. Danbatta, Precambrian crustal development in the northwestern part of Zuru schist belt, northwestern Nigeria, J. Min. Geol. 44 (1) (2008) 43–56, https://doi.org/10.4314/jmg.v44i1.18883.
[34] D.T. Thompson, EULDPH: a new technique for making computer-assisted depth estimates from magnetic data, Geophysics 47 (1) (1982) 31–37, https://doi.org/10.1190/1.1441278.
[35] A.B. Reid, J. Ebbing, S.J. Webb, Avoidable euler errors – the use and abuse of euler deconvolution applied to potential fields. European association of geoscientists & engineers, Geophys. Prospect. (2013) 1–7, https://doi.org/10.1111/1365-2478.12119.
[36] I.G. Odidi, A. Mallam, N. Nasir, Depth to magnetic sources determination using Source Parameter Imaging (SPI) of aeromagnetic data of parts of Central and North-Eastern Nigeria: a reconnaissance tool for geothermal exploration in the area, Sci. World J. 15 (3) (2020) 19–23.
[37] R.S. Smith, J.B. Thurston, T.F. Dai, I.N. MacLeod, SPITM the improved source parameter imaging method, Geophys. Prospect. 46 (2) (1998) 141–151, https://doi.org/10.1046/j.1365-2478.1998.00084.x.
[38] J.S. Adams, P. Gasparini, Gamma Ray Spectrometry of Rocks, Elsevier Publication Company, New York, 1970.
[39] A.B. Pires, Identficacao Geofisica de areas de alteracao hidrotermal, Crixas-Guarinos, Goias, Review Bras Geosciences 25 (1) (1995) 61–68.
[40] J.H. Galbraith, D.F. Saunders, Rock classification by characteristics of aerial gamma-ray measurements, J. Geochem. Explor. 18 (1) (1983) 47–73.
[41] S.O. Sanusi, J.O. Amigun, Logistic-based translation of orogenic gold forming processes into mappable exploration crite- ria for fuzzy logic mineral exploration targeting in the Kushaka schist belt North-central, Nigeria, Natural Resoures Research (2020), https://doi.org/10.1007/s11053-020-09689-1.
[42] N. Maden, E. Akaryali, Gamma ray spectrometry for rec- ognition of hydrothermal alteration zones related to a low sulfidation epithermal gold mineralization (eastern pontides, NE Turkiye), J. Appl. Geophys. 122 (2015) 74–85.
[43] B.L. Dickson, K.M. Scott, Interpretation of aerial gamma ray surveys-adding the geochemical factors, Journal of Austria Geology Geophysics 17 (2) (1997) 187–200.
[45] A.V. Efimov, Multiplikativiniyj pokazatel dlja vydelenija endogennych rud aerogamma-spectrometriceskim dannym in Metody rudnoj geofiziki, in: Lenigrad, Naucnoproizvodstvennoje Objedinenie. Geofizica, 1978, pp. 59–68.
[46] D.J. Isles, L.R. Rakin, Geophysical Interpretation of Aeromagnetic Data, Australian Society of Exploration Geophysicist (ASEG), Australia, 2013. http://www.aseg.org.au.